

# *In-situ* Data Analysis of Protein Folding Trajectories

Travis Johnston\*, Boyu Zhang\*, Adam Liwo<sup>†</sup>, Silvia Crivelli<sup>‡</sup>, Michela Taufer\*

November 3, 2021

## Abstract

The transition from petascale to exascale computers is characterized by substantial changes in the computer architectures and technologies. The research community relying on computational simulations is being forced to revisit the algorithms for data generation and analysis due to various concerns, such as higher degrees of concurrency, deeper memory hierarchies, substantial I/O and communication constraints. Simulations today typically save all data to analyze later. Simulations at the exascale will require us to analyze data as it is generated and save only what is really needed for analysis, which must be performed predominately *in-situ*, i.e., executed sufficiently fast locally, limiting memory and disk usage, and avoiding the need to move large data across nodes.

In this paper, we present a distributed method that enables *in-situ* data analysis for large protein folding trajectory datasets. Traditional trajectory analysis methods currently follow a centralized approach that moves the trajectory datasets to a centralized node and processes the data only after simulations have been completed. Our method, on the other hand, captures conformational information *in-situ* using local data only while reducing the storage space needed for the part of the trajectory under consideration. This method processes the input trajectory data in one pass, breaks from the centralized approach of traditional analysis, avoids the movement of trajectory data, and still builds the global knowledge on the formation of individual  $\alpha$ -helices or  $\beta$ -strands as trajectory frames are generated.

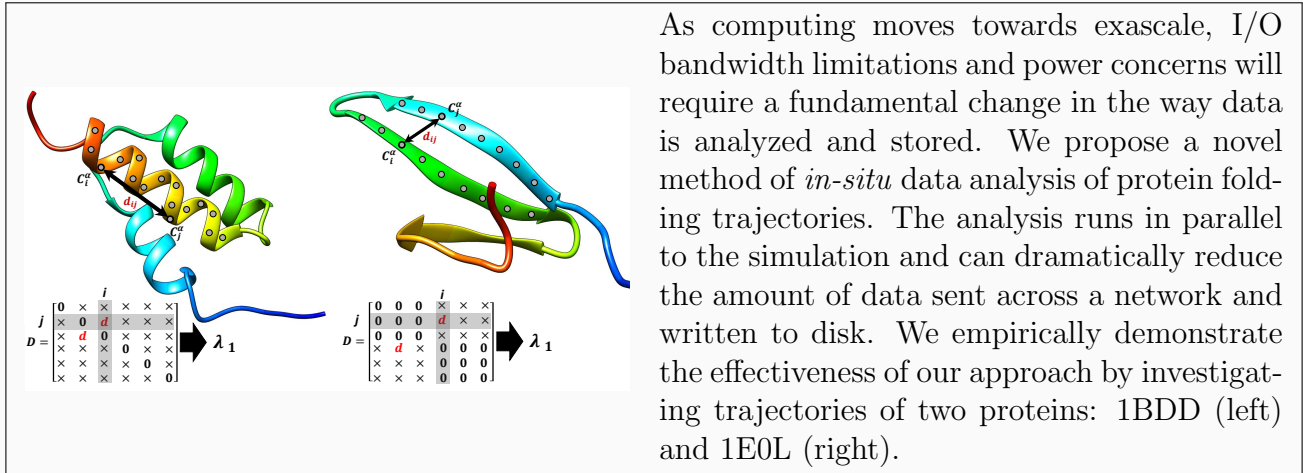
Keywords: exascale computing, I/O reduction, ensemble protein folding, eigenvalues ■

---

\*Department of Computer and Information Sciences, University of Delaware

<sup>†</sup>Department of Chemistry, University of Gdansk, Poland

<sup>‡</sup>Lawrence Berkeley National Laboratory



# INTRODUCTION

Fundamental changes in computer architecture will accompany the transition from petascale to exascale computing. Aspects like significantly higher concurrency, deeper memory hierarchies, substantial I/O and communication bottlenecks, and power constraints are forcing the community to revisit traditional algorithms. The higher degree of concurrency speeds the generation of simulation data but I/O and communication bottlenecks, as well as power constraints, severely limit data storage and movement. While simulations today save all the data to be analyzed later, simulations at the exascale will require us to analyze data as it is generated and save only what is really needed. New techniques are needed for the data analysis. When integrated in simulations, the analysis should be performed *in-situ*, i.e. execute sufficiently fast locally, use a small amount of memory and disk, and avoid substantial or frequent data movement<sup>1</sup>. In this paper we address the challenge of defining an *in-situ* data analysis for specific datasets: ensembles of trajectories in protein folding simulations. In past work we addressed a similar challenge for protein ligand docking simulations<sup>2-4</sup>. This work is an expansion and refinement of work on smaller proteins<sup>5</sup>; in particular, the method we present here is suitable for much larger proteins than in the previous work and provides a finer-grained, multi-faceted view of the protein conformations as they evolve through a simulation.

In protein folding simulations, a protein's string of amino acids connected by peptide bonds folds into a compact shape, called tertiary or native structure, which determines how the protein functions. An intermediate level between primary and tertiary structure is called secondary structure and it is composed of  $\alpha$ -helices,  $\beta$ -strands, and the turns and loops that connect them.  $\alpha$ -helices and  $\beta$ -strands involve well-understood local interactions via hydrogen bonding between neighboring amino acids.  $\beta$ -strands align and bond with other strands forming  $\beta$ -sheets. Molecular dynamics (MD) simulations aim to understand the properties of these dynamic systems at the atomic level by providing detailed information on the fluctuations and conformational changes as they fold.

The increase of computing power and the high degree of parallelism in the folding simulations enable unprecedented fine-grained time scales, and allow an increasingly large number

of trajectories to be computed in parallel. The analysis of these trajectories, on the other hand, is highly centralized, requiring major data movements that will no longer be sustainable on exascale machines. To reach any conclusion, traditional analyses initially move all the frame data to a parallel file system (e.g., Lustre or GPFS). Data are eventually moved to the user’s machine or a cluster dedicated to the analysis, requiring a second massive movement of data (see Figure 1).

The method we propose in this paper enables an *in-situ* analysis for large distributed trajectory datasets and removes the need for moving large amounts of data, thus better fitting with the profile of exascale machines. As shown in Figure 2, our method processes each frame locally and in isolation, transforms each protein conformation into metadata that is sensitive to conformational changes, and avoids the movement of trajectory data. This is a fundamental break from the centralized approach of traditional data analysis that still builds a global knowledge of the folding trajectory.

Specifically, as soon as a frame is generated, the frame is written to local storage and the metadata is generated and stored locally for the entire length of the simulation. Stable states are identified by regions of the trajectory where the metadata changes very little (i.e., they fluctuate around an average value). During these periods, one or several representative frames can be selected and moved from local storage to the parallel file system. The other frames that are similar can be removed from local storage without being written (moved) to the parallel file system. As new frames are generated, each frame’s metadata is computed and compared against the stored metadata. When new stable regions are detected, the process repeats: representative frames are chosen and moved from local storage to the persistent parallel file system. Transition states of the trajectory can be also identified as the metadata drifts away from average values; if these transition states are of interest to the researcher they can be moved to the parallel file system. By doing this, our method limits the amount of data stored on the local hard drive while maintaining the ability to compare new frames to old, since all metadata on local storage are preserved. As we will discuss in this paper, the map to metadata and comparison of metadata is very inexpensive computationally. Thus, we have a true *in-situ* data analysis which accomplishes our primary goal.

# METHODOLOGY

Our goal is to identify how trajectories, in ensemble folding simulations, evolve without the need for writing the entire trajectory to disk. We accomplish our goal by independently mapping each conformation to compact metadata. In order to be useful, the map to metadata must preserve conformational *closeness*. In other words, similar protein conformations must map to similar metadata. The metadata can be generated and analyzed *in-situ*. The result of the analysis determines which frames are ultimately written to disk for access after the completion of the simulation.

## Mapping a conformation to metadata

The map to metadata consists of three steps and is applied independently to each frame of the trajectory.

First, we discretize the protein by selecting (up to) two representative atoms per amino acid: the  $\alpha$ -carbon, which is the carbon in the amino acid backbone, and the  $\beta$ -carbon, which is the first carbon atom in the side chain. The amino acid Glycine is exceptional in that it contains no  $\beta$ -carbon; in this case, we select only one representative for that amino acid. The PDB files we used employed a coarse-grained representation; the CB entry in these PDB files gives the position of the side chain center. Throughout this paper we will refer to these entries as  $\beta$ -carbons, but the reader should keep in mind that these are actually side chain centers. We expect that in practice this choice makes little difference. We extract the position of each representative carbon as  $\vec{r}_1, \vec{r}_2, \dots, \vec{r}_n$  where  $\vec{r}_i = (x_i, y_i, z_i)$  is the Cartesian coordinate of the  $i^{\text{th}}$  representative carbon. Throughout the remainder of this section, we refer to  $n$  as the number of carbons selected in the discretization process. Note that  $n$  is approximately twice the number of amino acids and is significantly smaller than the total number of atoms in the entire protein.

Second, using the selected carbons' atomic coordinates, we create an  $n \times n$  distance matrix,  $D = [d_{ij}]$ , where  $d_{ij}$  records the square of the Euclidean distance between two carbon atoms, i.e.  $d_{ij} = \|\vec{r}_i - \vec{r}_j\|_2^2 = (x_i - x_j)^2 + (y_i - y_j)^2 + (z_i - z_j)^2$ . The matrix  $D$  is called a Euclidean distance matrix, or EDM.

Third, we compute the eigenvalues of the matrix  $D$ . The matrix  $D$  has three important properties that affect the eigenvalues.  $D$  is a symmetric, real matrix with non-negative entries and zeros along the diagonal. Because  $D$  is symmetric all of its eigenvalues are real. Since  $D$  is real and symmetric it is diagonalizable; this implies that  $D$  is similar to a diagonal matrix  $E$  containing the eigenvalues of  $D$ . The trace of  $D$  is clearly zero and the trace is similarity invariant; hence, the sum of the eigenvalues of  $D$  is zero. Finally, and most notably, because of the choice of distance measure, if  $n \geq 5$  and all of the carbon atoms do not lie on a common plane, then  $D$  has exactly 5 non-zero eigenvalues. We use non-zero eigenvalues of  $D$  to create a metadata packet associated with each frame.

While we could use all 5 non-zero eigenvalues, we focus exclusively on the largest eigenvalue. The reason for this is two fold. First, there is natural dependence among the eigenvalues. To see this, suppose that the non-zero eigenvalues of  $D$  are  $\lambda_5 \leq \lambda_4 \leq \dots \leq \lambda_1$ . Since the sum of the eigenvalues is 0 we can write:  $\lambda_5 + \lambda_4 + \lambda_3 + \lambda_2 = -\lambda_1$ . So, knowing 4 of the 5 eigenvalues is enough to determine the fifth. Second, our empirical observations show that the three non-zero eigenvalues with smallest magnitude are orders of magnitude smaller than the largest eigenvalue. We observe that the 5 non-zero eigenvalues satisfy:  $\lambda_5 < \lambda_4 < \lambda_3 < \lambda_2 < 0 < \lambda_1$ , and  $|\lambda_i| \ll \lambda_1$  for  $i = 2, 3, 4$ . This means that  $-\lambda_5 \approx \lambda_1$ . The result is that changes in  $\lambda_i$  for  $i = 2, 3, 4$  are nearly imperceptible and  $\lambda_5$  is highly correlated with  $\lambda_1$ .

We compute the eigenvalues of  $D$  by using standard libraries. Our code is written in Python and uses the linear algebra libraries available in `scipy` (SCientific PYthon). We use the function `scipy.linalg.eigh` which takes advantage of the symmetry of the matrix.

The method described above generates a piece of metadata representing the entire protein. In practice, it behaves as a very coarse view of the protein. In order to get finer grained detail and capture the formation of an individual  $\alpha$ -helix or  $\beta$ -strand, we modify the method to *zoom in* on a region of interest. Suppose we want to track the formation of an  $\alpha$ -helix (or  $\beta$ -strand) and we know that carbons  $i$  through  $j$  fold into an  $\alpha$ -helix (or  $\beta$ -strand). To focus on the individual structure, we consider an EDM,  $D_1$ , which is a submatrix of  $D$  corresponding to rows and columns  $i$  through  $j$ . One can equivalently view  $D_1$  as the EDM generated when one only considers the representative carbons that form the substructure. The matrix

$D_1$  has the same properties of the matrix  $D$  (i.e., symmetry, non-negativity) but has fewer rows and columns. Provided that  $j - i + 1 \geq 5$  and not all the coordinates represented in  $D_1$  are on a common plane, then  $D_1$  also has exactly 5 non-zero eigenvalues. These eigenvalues share the same properties as the eigenvalues of  $D$ ; hence we keep only the largest eigenvalue of  $D_1$ .

To study the relative shape and position of two substructures (e.g., two  $\alpha$ -helices or  $\beta$ -strands), we build a different matrix that is derived from  $D$ , but is no longer an EDM. Suppose that we have two  $\beta$ -strands which are forming and we want to track how they position themselves relative to each other while forming a  $\beta$ -sheet. The first  $\beta$ -strand includes carbons  $a_1, a_2, \dots, a_k$  and the second  $\beta$ -strand includes carbons  $b_1, b_2, \dots, b_\ell$ . We begin by constructing a (non-square) matrix  $C := [c_{ij}]$  where

$$c_{ij} := (x_{a_i} - x_{b_j})^2 + (y_{a_i} - y_{b_j})^2 + (z_{a_i} - z_{b_j})^2.$$

Then, the inter-structure *distance* matrix we create is the following:

$$D_2 := \left[ \begin{array}{c|c} 0 & C \\ \hline C^T & 0 \end{array} \right].$$

The matrix  $D_2$  is a submatrix of  $D$  with rows and columns  $a_1, \dots, a_k, b_1, \dots, b_\ell$ , and with entries  $d_{a_i a_j}$  and  $d_{b_i b_j}$  zeroed out. The entries  $d_{a_i a_j}$  are zeroed out to remove as much variation as possible from within a single structure.

The matrix  $D_2$  is not a EDM because there are zeros off the diagonal. However, it has all the essential properties of an EDM.  $D_2$  is real and symmetric which ensures that we have all real eigenvalues; it is also diagonalizable and  $\text{tr}(D_2) = 0$ . Furthermore, because of the block structure of  $D_2$  whenever  $\lambda$  is an eigenvalue of  $D_2$  so is  $-\lambda$ . With this observation in mind we only consider the positive eigenvalues of  $D_2$ . Additionally, one can prove that  $D_2$  has at most 5 positive eigenvalues; for the interested reader, the proof is contained in the appendix. Again, we select only the largest eigenvalue because the smaller eigenvalues tend to be much, much smaller.

Throughout the remainder of this paper we use the following naming convention when referring to matrices.  $D$  always refers to an EDM constructed using all the  $\alpha$ - and  $\beta$ -carbons

from the entire protein.  $D_i$  always refers to an EDM constructed using all the  $\alpha$ - and  $\beta$ -carbons from the  $i^{\text{th}}$  substructure ( $\alpha$ -helix, or  $\beta$ -strand).  $D_{ij}$  always refers to the block matrix we last discussed which compares the  $i^{\text{th}}$  substructure's relative position to the  $j^{\text{th}}$  substructure.

## **Eigenvalues preserve conformational closeness**

In the outset of this section, we asserted any choice of a map to metadata must preserve computational closeness in order to be useful. To be useful, we must be certain that if conformations are similar their metadata will also be similar; we also need to be certain that when we see disparate metadata that the originating conformations are also quite disparate. The eigenvalues of the matrices  $D$ ,  $D_i$ , and  $D_{ij}$  give us this guarantee. This is a result of the stability of eigenvalues<sup>6</sup>. The eigenvalues of a matrix are said to be stable if small perturbations in the matrix result in only small perturbations in the eigenvalues. Not all matrices have stable eigenvalues; however, real, symmetric matrices do have stable eigenvalues and we always consider real symmetric matrices. The change in conformation from one frame to another can be viewed as a perturbation. The second frame can be viewed as the first frame with some changes (perturbations) applied. If the conformations are very similar, then the perturbation is very small; as a consequence, the eigenvalues must, by stability, be close together. If the conformations are very different, then the perturbation will be very large. When the perturbation is large the change difference in eigenvalues can also be large. In principle, there is no guarantee that the difference in these eigenvalues will be large; however, in our experiments we did not observe cases where the conformations were quite different and the eigenvalues were quite similar.



# RESULTS

In this section we present empirical results that demonstrate the accuracy and efficiency of our method for *in-situ* data analysis of trajectories.

## Datasets

We consider two proteins: 1BDD and 1E0L. The native structures of these proteins were experimentally determined by NMR spectroscopy. The protein 1BDD consists of 60 amino acids and it is composed of a bundle of three  $\alpha$ -helices as shown in Figure 3. Helix 2 (Glu25-Asp37) and Helix 3 (Ser42-Ala55) are antiparallel to each other, and Helix 1 (Gln10-His19) is tilted with respect to the other two<sup>7</sup>. The protein 1E0L consists of 35 amino acids and it presents a triple-stranded antiparallel  $\beta$ -sheet topology<sup>8</sup> as shown in Figure 4.

Molecular dynamics simulations for 1BDD and 1E0L were carried out with the coarse-grained UNRES force field<sup>9-11</sup> using the parameterization for  $\alpha$ -helical<sup>12</sup> and  $\beta$ -sheet proteins<sup>13</sup>, respectively. The simulations were run at  $T = 300$  K. About 100,000,000 MD steps were run at the time step of 4.89 fs. Frames were collected every 5,000 steps. Langevin dynamics were applied scaling the water friction coefficient by a factor of 100 as in our earlier work<sup>14,15</sup>.

## Formation of individual structures

We first assess the ability of our method to identify the formation of individual secondary structures (i.e., a single  $\alpha$ -helix or a single  $\beta$ -strand). We compute the eigenvalues for the region of the protein that eventually forms the secondary structure being examined; these eigenvalues are associated to distance matrices of type  $D_i$  referenced in the methodology section.

We begin our study by examining a folding trajectory of the protein 1BDD which contains a bundle of 3  $\alpha$ -helices. The regions which fold into helices span 10, 13, and 14 amino acids respectively. The total number of  $\alpha$ - and  $\beta$ -carbons in each  $\alpha$ -helix is 20, 25, and 28 respectively. Thus, in the process of computing the eigenvalues for each folding helix, we consider three distance matrices per frame. Each matrix is relatively small:  $20 \times 20$ ,  $25 \times 25$ ,

and  $28 \times 28$  respectively. Note that each matrix easily fits in memory. We compute the largest eigenvalue of each of these matrices and store it as metadata.

Figure 5 shows to the formation of Helix 2 in the protein 1BDD. Figure 5.a (top) shows the evolution of the largest eigenvalue for this helix over the first 100 frames of the trajectory. Each point in the plot corresponds to the largest eigenvalue of the distance matrix  $D_2$  for a given frame. Figure 5.b (middle) shows the root-mean-squared deviation (RMSD) of the structure as compared to the corresponding native structure which had been determined using NMR spectroscopy. Looking at the largest eigenvalue sequence we see three stages. The first stage (blue) has the largest values and the most variability. The second stage (red) has much less variability. The final stage (green) is made up of smaller values and has less variability than the previous stages. We selected two frames from each region and visualized the corresponding conformation using Chimera<sup>16</sup> in Figure 5.c (bottom). The highlighted (cyan) portion of the protein corresponds to the region under consideration that eventually becomes Helix 2. We observe that in the first stage, the helix is completely unfolded. Throughout the second stage, the helix has begun to form and contains a single helical turn. By the third stage, the helix is much better formed and consists of several helical turns.

The construction of Helices 1 and 3 follows a similar behavior but, because one of their ends is loose, the substructures exhibit more variability and less stability. Figure 6 presents results related to the protein region that folds into Helix 3; the structure of the figure is similar to Figure 5: Figure 6.a (top) and Figure 6.b (middle) shows the largest eigenvalue and RMSD patterns and Figure 6.c (bottom) shows representative snapshots. The third helix forms very rapidly. We observed this formation in both the eigenvalue and RMSD patterns. We also see only two stages: the first stage before frame 67 and the second after frame 67. The sudden change in the eigenvalue pattern coincides with the sudden formation of the helix. In Figure 6.b we visualize three frames before and three frames after frame 67.

We observed that the trajectory of eigenvalues has a remarkably similar trajectory to the RMSD (comparing the shapes in Figure 5.a to Figure 5.b and comparing Figure 6.a to Figure 6.b). The important thing to note is that, in practice, RMSD values are measured against a known reference structure that is not always available. The computation of the

eigenvalues, on the other hand, is performed on a single frame in isolation (i.e., without looking at the previous or next frames).

The all- $\beta$  protein 1E0L is composed of three  $\beta$ -strands. The regions which fold into strands span 6, 7, and 5 amino acids respectively. The total number of  $\alpha$ - and  $\beta$ -carbon atoms considered in each strand is 12, 14, and 10 respectively. When we consider the distance submatrix used for the computation of eigenvalues, their sizes are  $12 \times 12$ ,  $14 \times 14$ , and  $10 \times 10$ . Figure 7, Figure 8, and Figure 9 refer to the first, second, and third  $\beta$ -strands respectively. Figure 7.a (top) shows the pattern of the largest eigenvalues obtained from the distance matrices composed of the  $\alpha$ - and  $\beta$ -carbon atoms of the first  $\beta$ -strand—one eigenvalue for each frame of the trajectory. We cluster the pattern in regions; each region’s values appeared to be stable. We hypothesize that these states are associated with metastable strands in the trajectory. From each cluster, three representatives are chosen by selecting frames whose  $\beta$ -strand’s eigenvalues are nearest the mean value of the eigenvalues in the region. The six sets of frames are visualized in Figure 7.b (bottom) using Chimera; frames that belong to the same cluster are grouped and boxed using the same color from the eigenvalue plot in Figure 7.a (top). In Figure 7 we see that within a cluster the highlighted region of the protein are mostly similar. The fourth cluster (blue) is a bit of an exception and is not as internally similar as the rest. Also, we notice that the second and fifth clusters (green and purple respectively) have both similar eigenvalues and a similar appearance.

Figure 8 and Figure 9 are structured similarly as Figure 7 but refer to the second and third  $\beta$ -strands respectively. The top of each figure presents the clustering of the largest eigenvalues for the considered  $\beta$ -strand; on the bottom we present the structures of three frames for each cluster that are selected because the  $\beta$ -strand’s eigenvalues are nearest the mean value of the eigenvalues in the associated cluster. Following the pattern for visualizing the first  $\beta$ -strand, we identify six clusters for the second strand and four clusters for the third strand. Again, we observe similarities among structures that are in the same cluster and have similar eigenvalues.

The visual analysis of similarities previously remarked in Figure 7, Figure 8, and Figure 9 is purely qualitative. In order to move from a qualitative and visual approach to a quantitative method to assess the similarities, we construct the heat maps for the three

$\beta$ -strands. The heat map is a visual representation of the RMSD of pairs of representative frames. Figure 10 shows the heat map for the first strand, Figure 11 for the second, and Figure 12 for the third. In these figures we compute the RMSD from the  $i^{\text{th}}$  representative  $\beta$ -strand to the  $j^{\text{th}}$  representative  $\beta$ -strand. The RMSD value is stored in the  $ij$  entry of a matrix. The matrix is visualized as a heat map where lighter (whiter) areas correspond to lower RMSD values (i.e., white being an RMSD of 0 Angstroms) and darker (redder) areas correspond to higher RMSD values. The heat map is blocked into regions by cluster.

Based on the conformation visualization in Figure 7 we expect the  $3 \times 3$  block diagonal portion of Figure 10 to be very lightly colored. We indeed observe this phenomena. The lightly colored block diagonal implies that conformations within a cluster have small RMSD and are therefore conformationally similar. Additionally, we confirm a visual observation about the second and fifth clusters being similar. This observation is reflected in the heat map in which we note that the blocks corresponding to Cluster 2 and Cluster 5 are nearly as light as the block diagonal. The other important feature of this heat map is that the  $3 \times 3$  blocks on the super-diagonal are quite dark colored. This indicates that when the eigenvalues significantly change resulting in a new cluster, the associated  $\beta$ -strand also significantly changes. Some of the most profound changes are observed between Clusters 1 and 2, and Clusters 3 and 4.

Figure 11 corresponds to the selected representatives of the second  $\beta$ -strand in Figure 8. For this strand, we observe many of the same features in the heat map as the visual analysis. Once again, the block diagonal is very light, as expected. Furthermore, we see from Figure 8 that the third and fourth clusters are visually similar as are the second and fifth. These observations are confirmed with the heat map.

Figure 12 is the heat map corresponding to the representatives of the third  $\beta$ -strand in Figure 9. We note one final observation: the eigenvalues from each strand settle into a final state at approximately the same time near frame 32000 in the simulation. This is likely a result of the interdependence of the strands. A single strand, by itself, is not very rigid; however, when the two strands are held together by hydrogen bonds, they are able to form a more rigid structure.

## Relative position of two substructures

In this section we assess the capability of our method to capture the relative position of a protein's secondary structures with respect to each other over the trajectory. Our empirical study considers once again an entire trajectory of the 1BDD protein with its three  $\alpha$ -helices. As a first view, we consider the largest eigenvalue of the distance matrix,  $D$ , formed by considering all the  $\alpha$ - and  $\beta$ -carbons. Then, to refine our view of the protein we consider the largest eigenvalues from the distance matrices for the individual helices (i.e., Helix 1, Helix 2, and Helix 3); these are the matrices of type  $D_i$  referenced in the methodology section. We also consider the largest eigenvalues from the matrices which compare distances between two helices at a time (i.e., Helix 1 with Helix 2, Helix 1 with Helix 3, and Helix 2 with Helix 3); these are the matrices of type  $D_{ij}$  referenced in the methodology section.

Examining the pattern of the largest eigenvalues for the entire protein in Figure 13.a (top) we observe a spike between Frames 1300 and 1400. When the spike occurs, the eigenvalue's magnitude is tripled. If we only considered this coarse grained view, all we can conclude is that during those frames, a structural change in the protein conformation happens but we are unable to pinpoint the precise cause.

To investigate the cause of the spike, we examined the three eigenvalue patterns associated to the distance matrices corresponding to an individual helix substructure. If there were a corresponding change in the eigenvalues, we could, for example, surmise that one or more of the helices may have unfolded and refolded again. Figure 13.b (middle) contains plots of these eigenvalues over the region of interest. We note that there are no significant changes in any of the eigenvalues over these ranges; thus we are led to conclude that the helix structure remained relatively unchanged over this portion of the trajectory. Finally, we consider the eigenvalues of the inter-structure distance matrices. When the relative positions of two rigid structures is constant there should be very little change in these matrices and hence, very little change in the corresponding eigenvalues. However, if two structures are moving either apart or together, we expect to see some significant changes in the associated distance matrix which manifests itself as significant changes in the eigenvalues. Figure 13.c (bottom) shows the largest eigenvalue of these inter-structure distance matrices. First, we notice that the

relative distance between Helix 1 and Helix 2 appears to change very little. On the other hand, we quickly observe that there is a prominent spike in the eigenvalues of the other two matrices comparing Helix 1 to Helix 3 and comparing Helix 2 to Helix 3. The common structure represented by those two matrices is Helix 3. We hypothesize that the explanation for the spike observed in the coarse view of the entire protein is a result of the third helix moving drastically with respect to the first and second helix. This hypothesis is confirmed when we view the conformations from the trajectory. Figure 14 shows consecutive frames between frames 1300 and 1400; Helix 3 (orange) swings away from Helix 1 and Helix 2 (cyan and magenta respectively) and then returns to its initial position. Note that the colors of the helices in this figure correspond to the coloring of the eigenvalues in Figure 13.b (middle). Over the course of this transformation, the changes in the relative position of the first two helices are small.

From these two case studies, of a 1BDD folding trajectory and a 1E0L folding trajectory, we observed two major strengths of our method. First, we were able to positively identify stable stages of both trajectories. We observed that during periods where the eigenvalues were stable the conformation was also stable. This bolsters our confidence in the ability to use distance between eigenvalues as an accurate proxy for the distance between conformations (typically measured with RMSD or similar metric). The most striking observation was the similarity in shape between RMSD and the largest eigenvalues that we saw in Figures 5.a-b and Figures 6.a-b. Second, we were able to leverage our ability to *zoom-in* on segments of the protein, and to compare two segments, to better understand the clues we saw at a coarse scale. The ability to view the protein from multiple angles proved useful to analyze the cause of the spike we saw in Figure 13.

# DISCUSSION

In this section we verify that our analysis is indeed an *in-situ* data analysis. We discuss the novelty of our approach and compare it with popular existing approaches. We conclude the section with a discussion of the challenges and opportunities related to integrating our method into existing tools for simulation and analysis.

## The cost of our in-situ data analysis

In order to be considered an *in-situ* data analysis, the CPU and memory footprint must be light enough to not interfere with the ongoing simulation and communication must be minimal. We note that our method does not communicate any information across the network, so its communication footprint is nonexistent.

Beginning with the trajectory for 1E0L (39130 frames, 35 amino acids) we construct 7 matrices for each frame (i.e., one matrix for the entire protein, one matrix for each of the three  $\beta$ -strands, and one matrix for each of the pairs of  $\beta$ -strands). Using a single CPU core running at 2.66 Ghz, it took 768.059s to compute all the eigenvalues; this implies an average CPU time of 0.0196s per frame. During a typical simulation, frames are generated using many cores of the node at a rate of about 6 seconds per frame; the 0.0196s on a single CPU is a negligible fraction of this time. The process of computing the eigenvalues required approximately 100 KB of memory. Finally, storing in memory the largest eigenvalue from each of the 7 matrices for the entire length of the trajectory requires about 2.2 MB memory.

The footprint is similarly light for the trajectory of 1BDD (41896 frames, 60 amino acids). The construction of the 7 matrices for the entire trajectory required 1417.651s implying an average CPU time of .0338s per frame. The matrices are somewhat larger and therefore require a little additional memory. The computation used approximately 200 KB of memory. Storing the largest eigenvalue (for 1BDD or 1E0L) requires the same amount of memory per frame,  $7 \times 8 = 56$  Bytes per frame, or about 2.35 MB for the entire trajectory.

We see that, both memory and CPU utilization are minimal with the proteins we considered. Thus, our analysis is an *in-situ* data analysis. Proteins with more substructures of interest require storing more eigenvalues. For example, if the protein has 10 substructures,

then there are up to 56 eigenvalues per frame (i.e., 1 eigenvalue for the matrix  $D$ , 10 matrices of the form  $D_i$  contribute 1 eigenvalue each, and 45 matrices of the form  $D_{ij}$ ), or a total of about 18 MB. This is still an insignificant amount of memory to be used. A further memory reduction can be achieved by storing the eigenvalues as single precision floating point numbers instead of double precision; this cuts the memory requirement in half with negligible loss of accuracy.

## The novelty of our approach

There are a number of methods that have been used to analyze trajectory data. One method, that works in a parallel distributed fashion is a framework called HiMach<sup>17</sup>. This framework is a MapReduce style interface that takes advantage of naturally parallel analysis operations to understand statistical data of long trajectories. Our work differs in that we focus on the similarity or discrepancy in the geometric structure of the conformation and not on any statistical information about the frame.

More sophisticated trajectory analyses, like those of Best et al.<sup>18</sup> and Phillips et al.<sup>19</sup> are traditionally centralized, and are therefore limited by the length of the trajectory and the size of the protein. These traditional methods also make comparisons to an energy minimal structure known ahead of time. Their works focus on constructing a frame-by-frame dissimilarity matrix and making reductions to lower dimensionality. Our work differs in that our analysis is not centralized and requires no data movement; our analysis is accomplished as the simulation runs (not post simulation); we require no *a priori* knowledge of an energy minimal structure; and, we are able to consider much larger proteins because we focus on smaller substructures.

The idea of mapping to metadata and analyzing the metadata is not new. Our previous work<sup>4</sup>, which explored protein-ligand docking, mapped ligand geometries to metadata using a sequence of projections and regression. In that work, the orientation of the ligand (both translation and rotation) is important; the analysis of metadata is done after the simulation and on the entire set of metadata. Our present work is different because we analyze the metadata during the simulation. In addition, our choice of metadata differs because the orientation of the protein (translation and rotation) is irrelevant; we need (and construct)



metadata that is rotation and translation insensitive.

We have previously developed a method to analyze protein folding trajectories<sup>5</sup>. Our earlier work involved map to metadata that is very similar to the work in this paper. The primary difference is that previously, we computed eigenvalues of a different matrix (not a Euclidean distance matrix) and we only considered a *coarse* view of the protein (building the matrix from all  $\alpha$ - and  $\beta$ -carbons). We were able to show that the method could identify stable states, but only in relatively simple proteins. And, without looking at matrices built from substructures, we were unable to get a fine-grained view of what was happening in the trajectory—we were only able to detect meta-stable and transition states. Our new approach gives us a much more refined view of the protein allowing us to extract more information about the conformational evolution.

## Opportunities to adopt and expand our method

We demonstrated that our method effectively captures conformational changes in proteins and that the metadata generated can be used to deduce what is happening in the trajectory without the need for moving the trajectory data and visualizing it.

In order to fully realize the potential of our method, it must be used as the simulation is running and the ensemble of trajectories across the compute nodes evolve. We envision the incorporation of our method into an existing framework for *in-situ* data analysis such as DataSpaces<sup>20</sup> and the tools for analysis being incorporated into well-known toolkits such as MMTSB<sup>21</sup>.

The analyses of eigenvalue patterns presented in this paper are performed manually. The scalability of our approach can be assured by extending our method and integrating automatic clustering algorithms that classify the trajectory state into either stable or transitional states based on the eigenvalue pattern. There are several popular methods for clustering data including centroid-based clustering (e.g. fuzzy *c*-means), density-based clustering (e.g. DBSCAN), and divide-and-conquer strategies making repeated use of fuzzy *c*-means, and others. To achieve maximum utility and to scale to large-scale simultaneous on thousands of nodes, it is necessary to integrate machine learning algorithms which intelligently, and automatically, detect the changes between these two states.

Finally, in this paper we focus entirely on *in-situ* data analysis. It is easy to envision transforming our method into an *in-transit* data analysis to cross compare large ensembles of trajectories evolving in parallel. In this case, the eigenvalue metadata is communicated to a central node for an ensemble analysis. The *in-transit* analysis is tasked with keeping track of which trajectories or substructures are rapidly evolving. The filtered knowledge can be ultimately used by the scientist to tune many simultaneous simulations on the fly (e.g., terminating simulations that quickly converged to a folded protein).

## CONCLUSIONS

As computing moves towards exascale the concurrency of supercomputers is increasing dramatically; however, because of power constraints the I/O bandwidth is essentially unchanged. The increase in concurrency makes it possible to run ever larger ensembles of protein folding simulations. These large ensemble simulations are capable of generating data faster than it can be written to disk, causing the movement of data to disk to substantially slow down the simulations. Traditional analyses of trajectory data do not scale on exascale machines because they rely on storing the entire generated datasets to disk first, and moving the data to a centralized node or dedicated cluster after the simulation is completed.

Our method of *in-situ* data analysis makes it possible to scale ensemble protein folding simulations in such a way to take full advantage of the increasing concurrency of these future machines by mapping each conformational frame in isolation into one or multiple eigenvalues. The eigenvalues serve as metadata for the trajectory analysis. We empirically demonstrate that, as a direct result of eigenvalue stability, our choice of metadata captures conformational changes for two different proteins: 1BDD and 1E0L composed of a bundle of three  $\alpha$ -helices and a triple-stranded antiparallel  $\beta$ -sheet topology respectively. Dealing with eigenvalues and using their pattern locally to select relevant frames to save to disk, we can significantly reduce the data movement during simulations. The eigenvalues can be ultimately used to monitor the transition of protein structures to stable states on the fly, without the need for the scientist to move entire trajectories to local disk and analyze them after the simulations are completed.

## ACKNOWLEDGMENTS

This work is supported by NSF grants #CCF-1318445/1318417. The authors gratefully acknowledge the use of Chimera for each of the visualizations of protein conformations presented in this paper and for the computation of RMSD. Chimera is developed by the Resource for Biocomputing, Visualization, and Informatics at the University of California, San Francisco (supported by NIGMS P41-GM103311). The authors thank Ms. Agnieszka Lipska, Faculty of Chemistry, University of Gdansk, for supplying the coarse-grained UNRES trajectories of protein A and FBP-28 WW domain; Adam Liwo acknowledges the support of Grant DEC-2013/10/M/ST4/00640 from the Polish National Science Center.

# APPENDIX

## The number of positive eigenvalues matrices $D_{ij}$

**Proposition.** *The matrix  $D_{ij}$  has at most 5 positive eigenvalues.*

*Proof.* First, we note that  $D_{ij}$  can be viewed as a *transformed* Euclidean distance matrix. Specifically, let  $D$  be the Euclidean distance matrix formed using all the selected atoms from the two structures represented by  $D_{ij}$ . In block form,  $D$  can be decomposed as

$$D = \left[ \begin{array}{c|c} A_{ii} & A_{ij} \\ \hline A_{ji} & A_{jj} \end{array} \right]$$

where  $A_{ii}$  contains distances between two points in structure  $i$ ,  $A_{jj}$  contains distances between two points in structure  $j$ , and  $A_{ji} = A_{ij}^T$  contains distances between one point in structure  $i$  and one point in structure  $j$ . By construction,  $D_{ij}$  has the form:

$$D_{ij} := \left[ \begin{array}{c|c} 0 & A_{ij} \\ \hline A_{ji} & 0 \end{array} \right].$$

With *slight* abuse of notation, let us say that  $A_{ij}$  as  $i$  rows and  $j$  columns and hence  $D$  and  $D_{ij}$  have  $i + j$  rows and columns. Let  $r_k$  be the  $k^{\text{th}}$  row of  $D$  and let  $r'_k$  be the corresponding  $k^{\text{th}}$  row of  $D_{ij}$ .

Because of the block structure of  $D_{ij}$  whenever  $\lambda$  is an eigenvalue of  $D_{ij}$  so is  $-\lambda$ . Thus, to show that  $D_{ij}$  has at most 5 positive eigenvalues, it suffices to show that  $D_{ij}$  has at most 10 non-zero eigenvalues. We recall that since  $D$  is a Euclidean distance matrix of a 3-dimensional object that  $D$  has at most 5 non-zero eigenvalues. Thus,  $D$  has rank (at most) 5 and consequently at most 5 rows of  $D$  can be linearly independent. We also note that it is clear that any row  $r'_k$  with  $k > i$  is linearly independent of the set of rows  $\{r'_1, r'_2, \dots, r'_i\}$ .

We will now show that at most 5 rows of  $\{r'_1, \dots, r'_i\}$  can be linearly independent. To do this, we need only show that any 6 of those rows are linearly dependent. Without loss of generality, we can assume those rows are  $r'_1, r'_2, \dots, r'_6$ . Since  $D$  has rank at most 5 we know that  $r_1, \dots, r_6$  are linearly dependent. Thus, there exist  $\alpha_1, \dots, \alpha_6$  (not all zero) so that

$$\alpha_1 r_1 + \alpha_2 r_2 + \dots + \alpha_6 r_6 = 0.$$

It follows that the same choice of coefficients yields:

$$\alpha_1 r'_1 + \alpha_2 r'_2 + \dots + \alpha_6 r'_6 = 0.$$

This is most easily seen when we think about the vectors  $r_k$  and  $r'_k$  coordinate-wise. For coordinates  $1, \dots, i$  the vectors  $r_k$  and  $r'_k$  have the same (non-zero) value. But, because  $\alpha_1 r_1 + \alpha_2 r_2 + \dots + \alpha_6 r_6 = 0$  it follows that, in the second sum, that coordinate is zero. In the remaining coordinates  $i + 1, i + 2, \dots, i + j$  all the entries of  $r'_k$  are zero, hence any choice of  $\alpha$  would result in zeros in these coordinates. Thus  $\alpha_1 r'_1 + \alpha_2 r'_2 + \dots + \alpha_6 r'_6 = 0$  as claimed and these 6 rows are linearly dependent. By a similar argument, any 6 rows of  $\{r'_{i+1}, \dots, r'_{i+j}\}$  are linearly dependent. Thus,  $D_{ij}$  has at most 10 linearly independent rows;  $D_{ij}$  has rank at most 10; and, therefore,  $D_{ij}$  has at most 10 non-zero eigenvalues.  $\square$

## References

1. J. Bennett, H. Abbasi, P.-T. Bremer, R. Grout, A. Gyulassy, J. Tong, S. Klasky, H. Kolla, M. Parashar, V. Pascucci, et al., In Proceedings of the 2012 ACM/IEEE International Conference for High Performance Computing, Networking, Storage and Analysis (SC'12), pp. 1–9 (2012).
2. T. Estrada, B. Zhang, P. Cicotti, R. Armen, and M. Taufer, *Comp. in Bio. and Med.* **42**, 758 (2012).
3. B. Zhang, T. Estrada, P. Cicotti, and M. Taufer, In the Proceedings of the 16<sup>th</sup> IEEE International Conference on Computational Science and Engineering, pp. 117–124 (2013).
4. B. Zhang, T. Estrada, P. Cicotti, P. Balaji, and M. Taufer, In Proceedings of the 15<sup>th</sup> IEEE/ACM International Symposium on Cluster, Cloud and Grid Computing, pp. 817–822 (2015).
5. B. Zhang, T. Estrada, P. Cicotti, and M. Taufer, In Proceedings of the 28<sup>th</sup> IEEE International Parallel and Distributed Processing Symposium, pp. 221–230 (2014).
6. T. Tao, *Poincaré's Legacies, Part II, pages from year two of a mathematical blog* (American Mathematical Society, 2009), chap. 1.5 When are eigenvalues stable?
7. H. Gouda, H. Torigoe, A. Saito, M. Sato, Y. Arata, and I. Shimada, *Biochemistry* **31**, 9665 (1992).
8. M. J. Marcias, V. Gervais, C. Civera, and H. Oschkinat, *Nat. Struct. Biol.* **7**, 375 (2000).
9. A. Liwo, C. Czaplewski, S. Ołdziej, A. V. Rojas, R. Kaźmierkiewicz, M. Makowski, R. K. Murarka, and H. A. Scheraga, in *Coarse-Graining of Condensed Phase and Biomolecular Systems*, edited by G. Voth (CRC Press, 2008), chap. 8, pp. 1391–1411.
10. A. Liwo, Y. He, and H. A. Scheraga, *Phys. Chem. Chem. Phys.* **13**, 16890 (2011).
11. M. Baranowski, C. Czaplewski, E. Golas, Y. He, D. Jagiel, P. Krupa, A. Liwo, G. Maisuradze, M. Makowski, M. Mozolewska, et al., in *Coarse-Grained Modeling of Biomolecules*, edited by G. Papoian (Crc Pr I Llc, 2016), p. in press.

12. A. Liwo, M. Khalili, C. Czaplewski, S. Kalinowski, S. Ołdziej, K. Wachucik, and H. Scheraga, *J. Phys. Chem. B* **111**, 260 (2007).
13. A. Liwo, C. Czaplewski, S. Ołdziej, U. Kozłowska, M. Makowski, S. Kalinowski, R. Kaźmierkiewicz, H. Shen, G. Maisuradze, and H. A. Scheraga, in *NIC Series, NIC Symposium 2008, 20-21 February 2008, Jülich, Germany*, edited by D. W. G. Münster and M. Kremer (John von Neumann Institute for Computing (NIC), 2008), vol. 39, pp. 63–70.
14. A. Liwo, M. Khalili, and H. A. Scheraga, *Proc. Natl. Acad. Sci. U.S.A.* **102**, 2362 (2005).
15. M. Khalili, A. Liwo, A. Jagielska, and H. A. Scheraga, *J. Phys. Chem. B* **109**, 13798 (2005).
16. E. F. Pettersen, T. D. Goddard, C. C. Huang, G. S. Couch, D. M. Greenblatt, E. C. Meng, and T. E. Ferrin, *J. Comput. Chem.* **25(13)**, 1605 (2004).
17. T. Tu, C. A. Rendleman, D. W. Borhani, R. O. Dror, J. Gullingsrud, M. O. Jensen, J. L. Klepeis, P. Maragakis, P. Miller, K. A. Stafford, et al., pp. 1–12 (2008).
18. C. Best and H. C. Hege, *Computing in Science Engineering* **4**, 68 (2002).
19. J. Phillips, M. Colvin, and S. Newsam, *BMC Bioinformatics* **12**, 445 (2011).
20. C. Docan, M. Parashar, and S. Klasky, in *Proceedings of the 19th ACM International Symposium on High Performance Distributed Computing (ACM, 2010)*, HPDC '10, pp. 25–36.
21. M. Feig, J. Karanicolas, and C. L. Brooks, *J Mol Graph Model* **22**, 377 (2004).



Figure 1: Traditional centralized data analysis. A single trajectory is computed on one node which writes all of its data to the parallel file system. Many hundreds or thousands of trajectories can be computed in parallel; each node writes all of its data to the parallel file system simultaneously.

Figure 2: *In-situ* data analysis in our proposed method. Each frame is converted into one or multiple eigenvalues in isolation. The eigenvalues pattern is used to select the frames to store to disk.

Figure 3: Native structure of protein 1BDD. The protein consists of 60 amino acids and it is composed of a bundle of three  $\alpha$ -helices. Helix 2 (Glu25-Asp37) and Helix 3 (Ser42-Ala55) are antiparallel to each other, and Helix 1 (Gln10-His19) is tilted with respect to the other two.

Figure 4: Native structure of protein 1E0L. The protein consists of 35 amino acids and it presents a triple-stranded antiparallel  $\beta$ -sheet topology.

Figure 5: Formation of the second (middle) helix of the protein 1BDD. The largest eigenvalue of the distance matrix corresponding to this substructure is plotted above and, for comparison, the RMSD for each frame is shown below. The RMSD is measured against a reference structure; only the region corresponding to the helix is considered. Below are representative conformations from each of the colored regions. The highlighted (cyan) portion of the protein corresponds to the region under consideration that eventually becomes the second helix.

Figure 6: Formation of the third helix of the protein 1BDD. The largest eigenvalue of the distance matrix corresponding to this substructure is plotted above and, for comparison, the RMSD for each frame is shown below. The RMSD is measured against a reference structure; only the region corresponding to the helix is considered. Below are representative conformations from each of the colored regions. The highlighted (cyan) portion of the protein corresponds to the region under consideration that eventually becomes the second helix.

Figure 7: Largest eigenvalue of the distance matrix for each frame of the trajectory. The distance matrix corresponds to the region that will become the first  $\beta$ -strand. Colored regions, clusters, represent expected *meta stable* states. From each cluster, three representatives are chosen. Each frame chosen as a representative is visualized below the eigenvalue plot. The region of the first  $\beta$ -strand is highlighted in cyan.

Figure 8: Largest eigenvalue of the distance matrix for each frame of the trajectory. The distance matrix corresponds to the region that will become the second  $\beta$ -strand. Colored regions, clusters, represent expected *meta stable* states. From each cluster, three representatives are chosen. Each frame chosen as a representative is visualized below the eigenvalue plot. The region of the first  $\beta$ -strand is highlighted in cyan.

Figure 9: Largest eigenvalue of the distance matrix for each frame of the trajectory. The distance matrix corresponds to the region that will become the third  $\beta$ -strand. Colored regions, clusters, represent expected *meta stable* states. From each cluster, three representatives are chosen. Each frame chosen as a representative is visualized below the eigenvalue plot. The region of the first  $\beta$ -strand is highlighted in cyan.

Figure 10: RMSD for each pair of representatives selected in Figure 7 and record this value in a matrix. The  $ij$ 'th entry is the RMSD between representative  $i$  and representative  $j$ . When computing the RMSD, we consider only the highlighted region of the protein. The matrix is colored so that lighter (whiter) colors correspond to smaller RMSD and darker (redder) colors correspond to larger RMSD.

Figure 11: RMSD for each pair of representatives selected in Figure 8 and record this value in a matrix. The  $ij$ 'th entry is the RMSD between representative  $i$  and representative  $j$ . When computing the RMSD, we consider only the highlighted region of the protein. The matrix is colored so that lighter (whiter) colors correspond to smaller RMSD and darker (redder) colors correspond to larger RMSD.

Figure 12: RMSD for each pair of representatives selected in Figure 9 and record this value in a matrix. The  $ij$ 'th entry is the RMSD between representative  $i$  and representative  $j$ . When computing the RMSD, we consider only the highlighted region of the protein. The matrix is colored so that lighter (whiter) colors correspond to smaller RMSD and darker (redder) colors correspond to larger RMSD.

Figure 13: Largest eigenvalue of all three types of matrices we consider. The top plot shows the largest eigenvalue of the distance matrix formed from the entire protein (1BDD). The middle row of plots show the largest eigenvalue of the distance matrix formed by individual substructures (regions that become helices). The color of the plot corresponds to the similarly colored region of the protein in Figure 14. The bottom row of plots show the largest eigenvalue of the inter-structures distance matrix formed by looking at two helices. There is a large change in the top plot between frames 1300 and 1400. There is no corresponding change in the individual structure plots (middle row); but we observe corresponding large changes in two of the three inter-structure plots.

Figure 14: Selected conformations of protein 1BDD frames 1300-1410. We observe that the third (orange) helix swings away from the other two helices, and then folds back together. This movement was captured by the eigenvalues recorded in Figure 13.

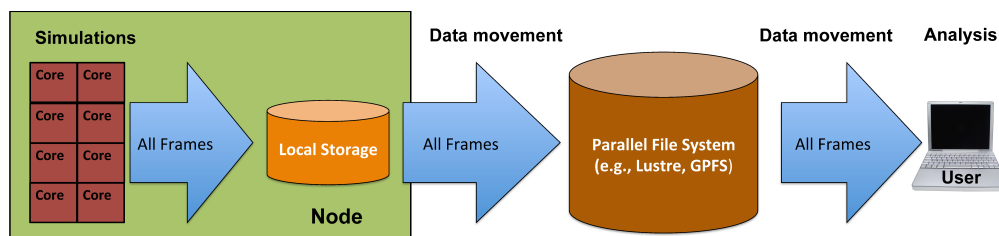


Figure 1  
 Johnston, Zhang, Liwo, Crivelli, and Taufer  
 J. Comput. Chem.

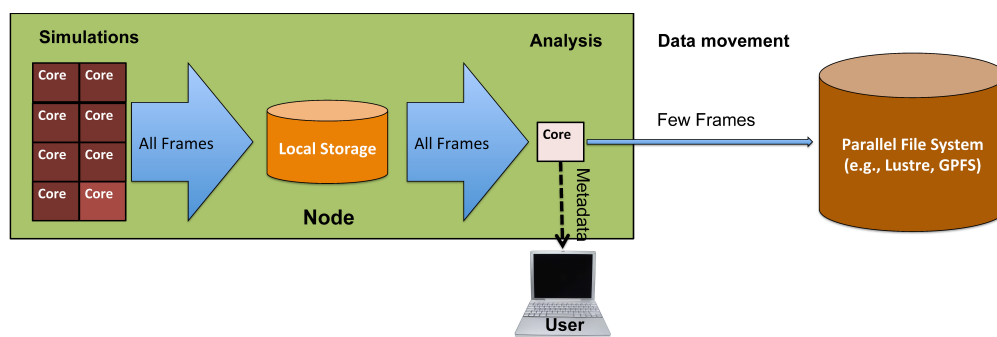


Figure 2  
 Johnston, Zhang, Liwo, Crivelli, and Taufer  
 J. Comput. Chem.

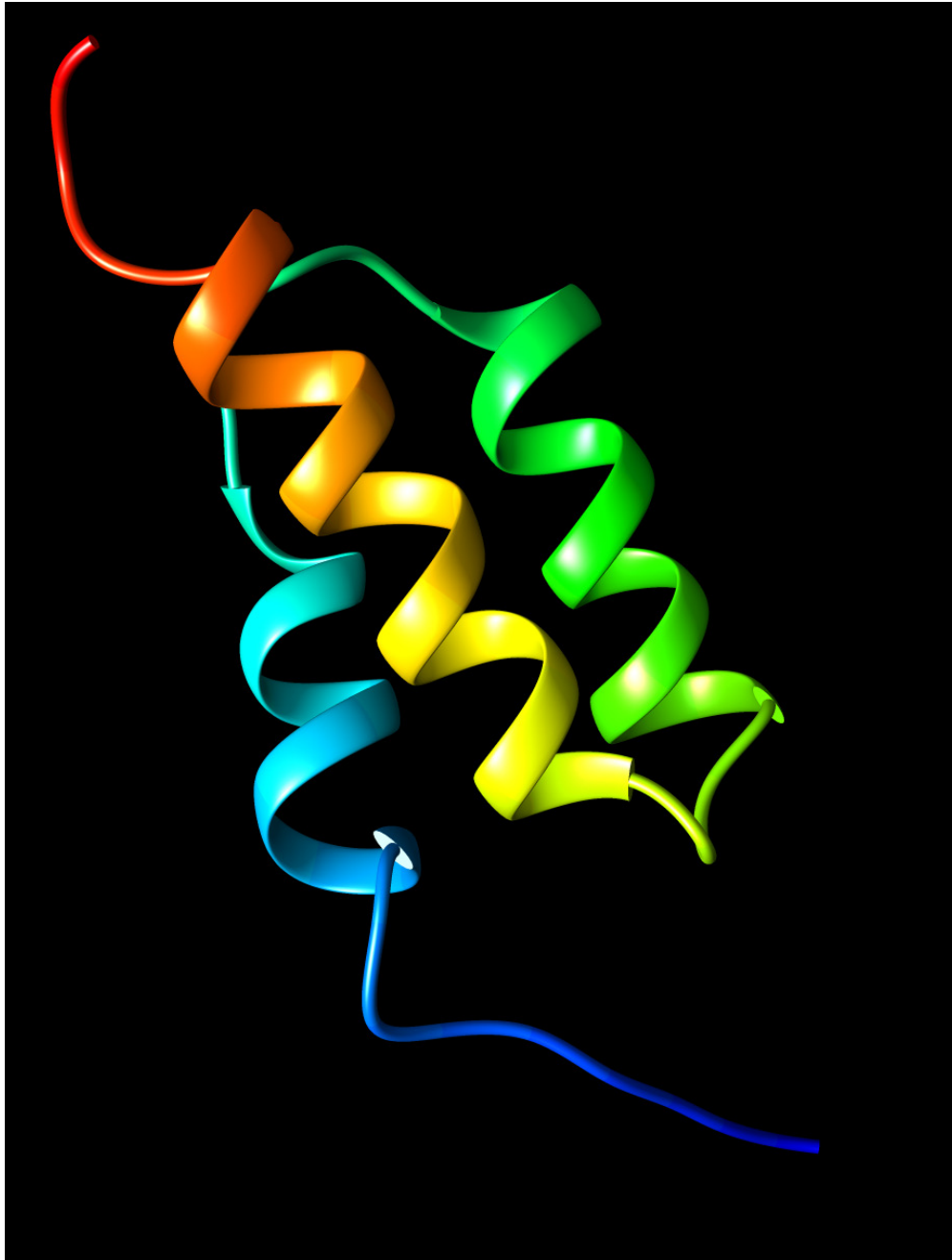


Figure 3  
Johnston, Zhang, Liwo, Crivelli, and Taufer  
*J. Comput. Chem.*

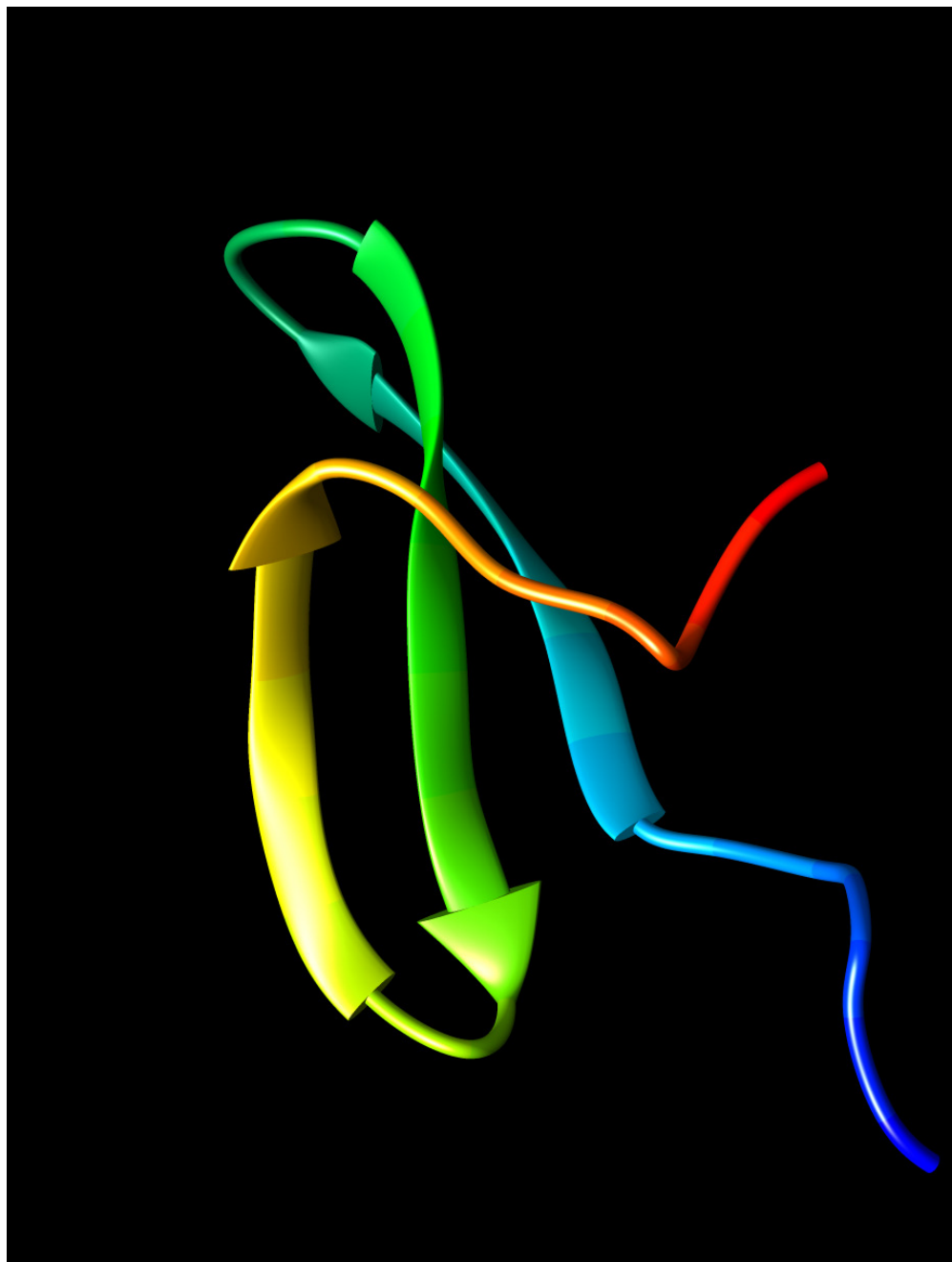
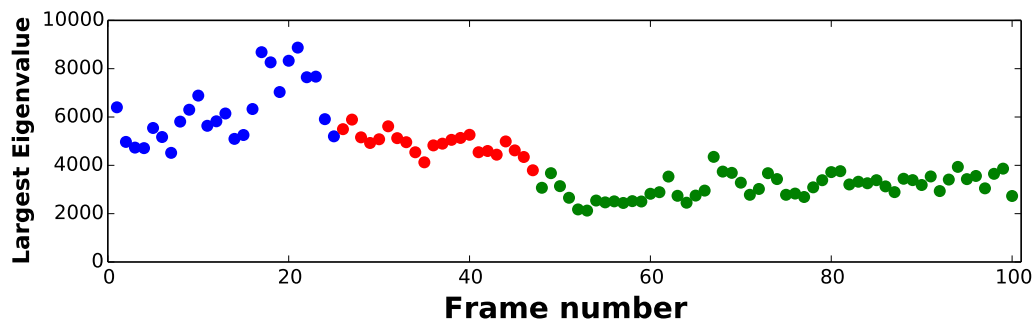
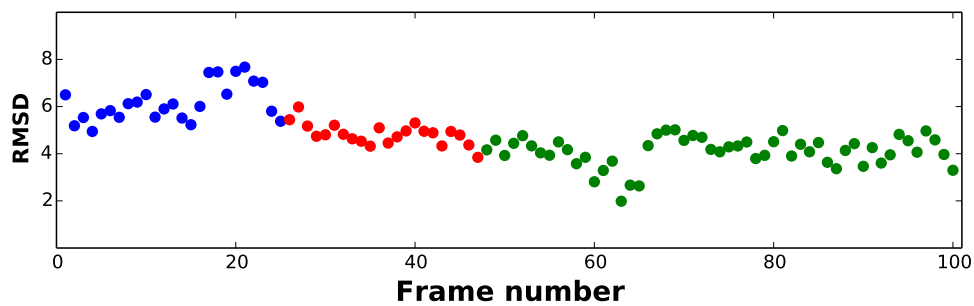


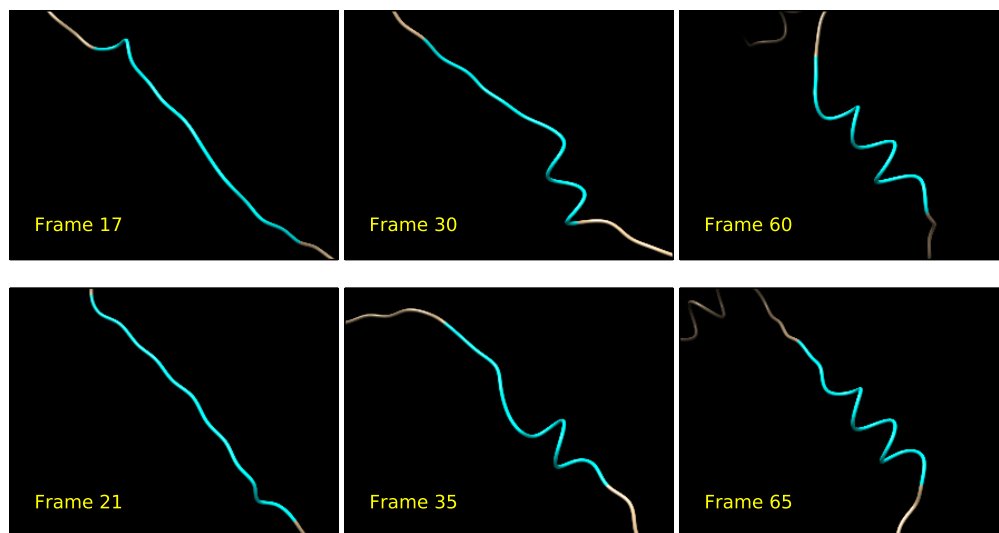
Figure 4  
Johnston, Zhang, Liwo, Criv-  
elli, and Taufer  
J. Comput. Chem.



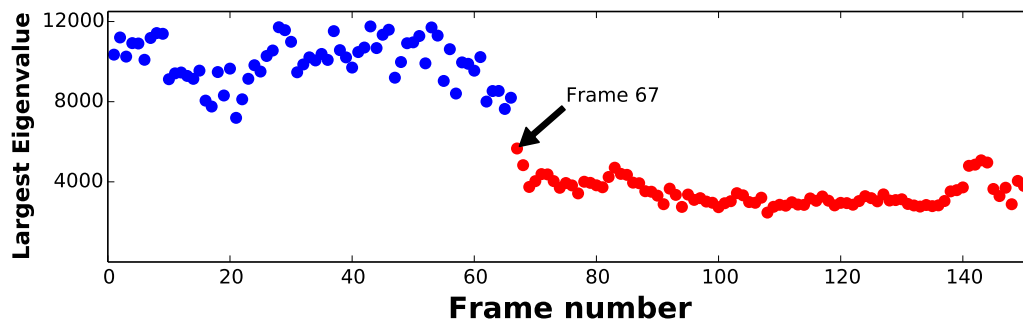
(a)



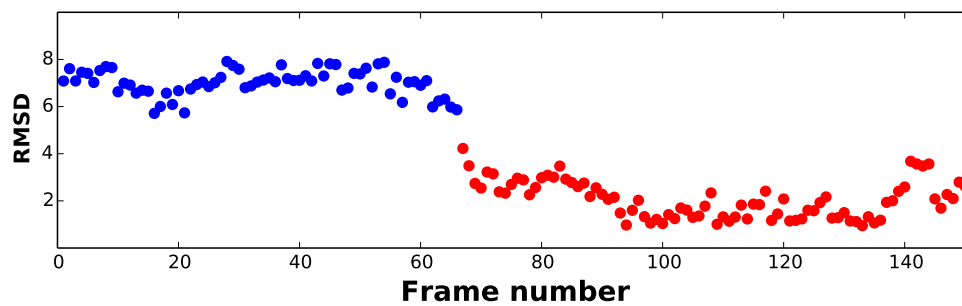
(b)



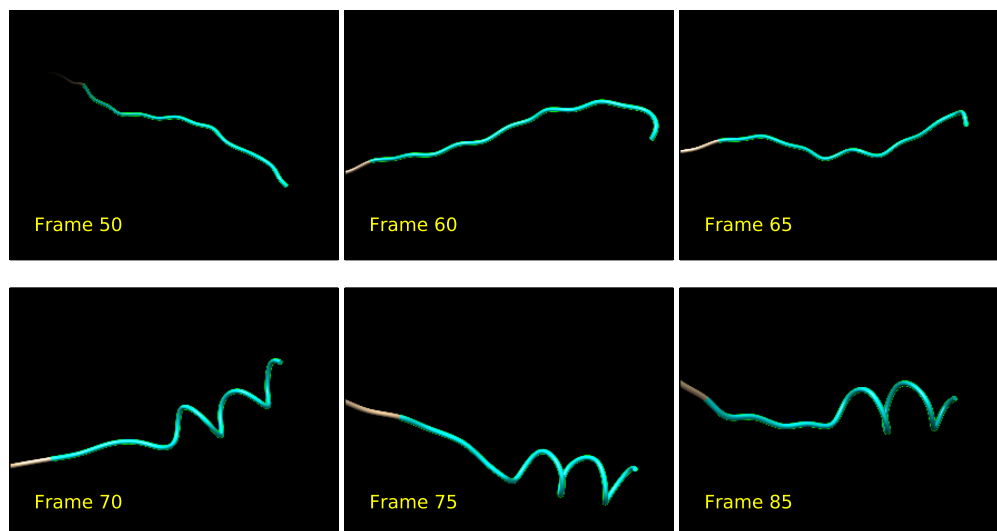
(c)  
 Figure 5  
 Johnston, Zhang, Liwo, Crivelli, and Taufer  
 J. Comput. Chem.



(a)

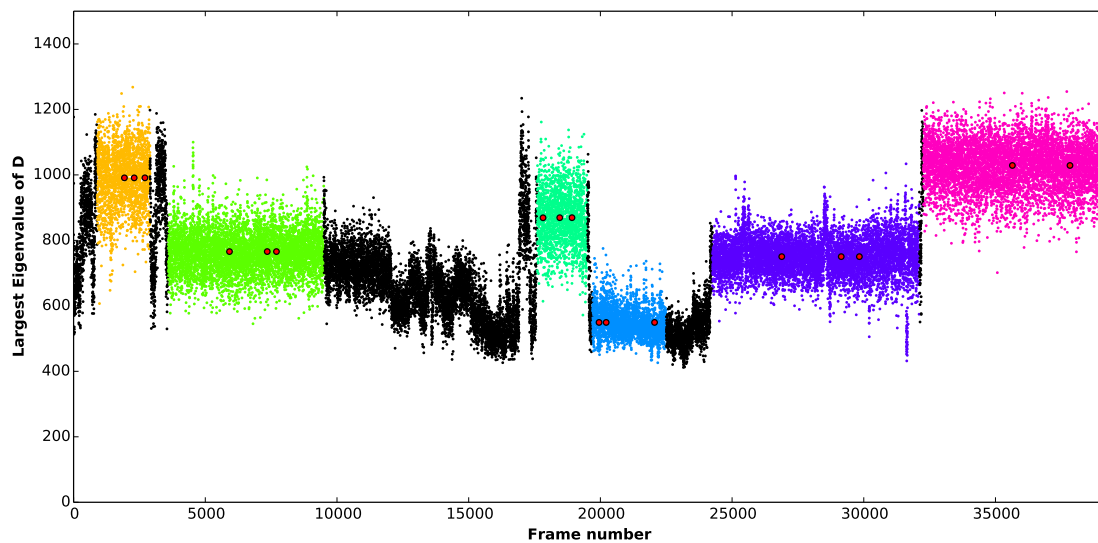


(b)

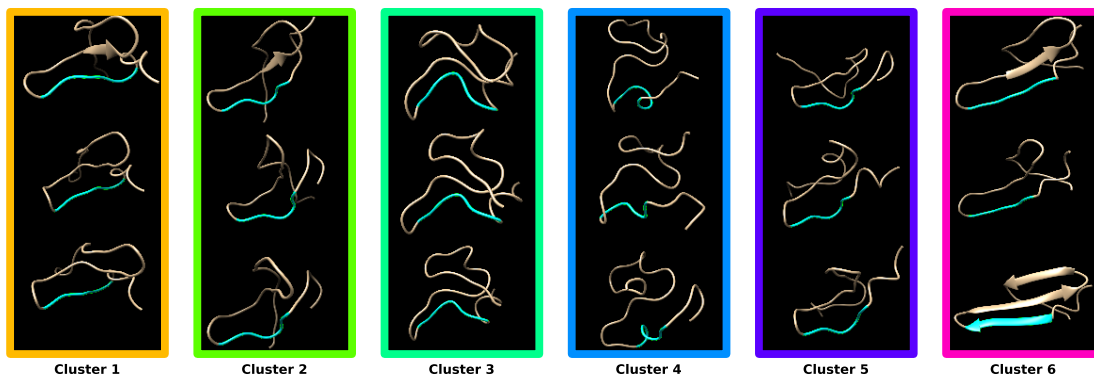


(c)  
 Figure 6  
 Johnston, Zhang, Liwo, Crivelli, and Taufer  
 J. Comput. Chem.



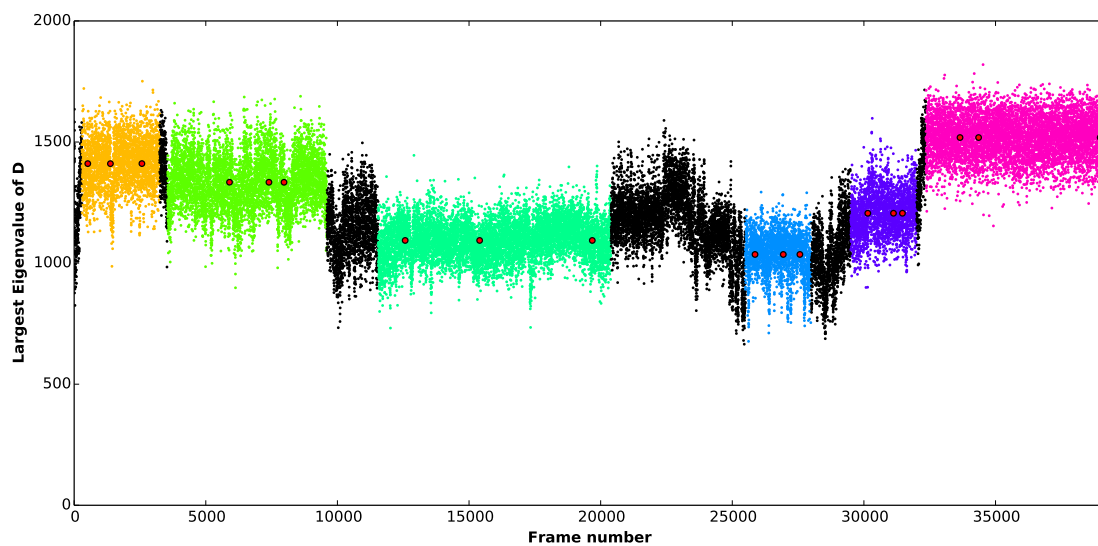


(a)

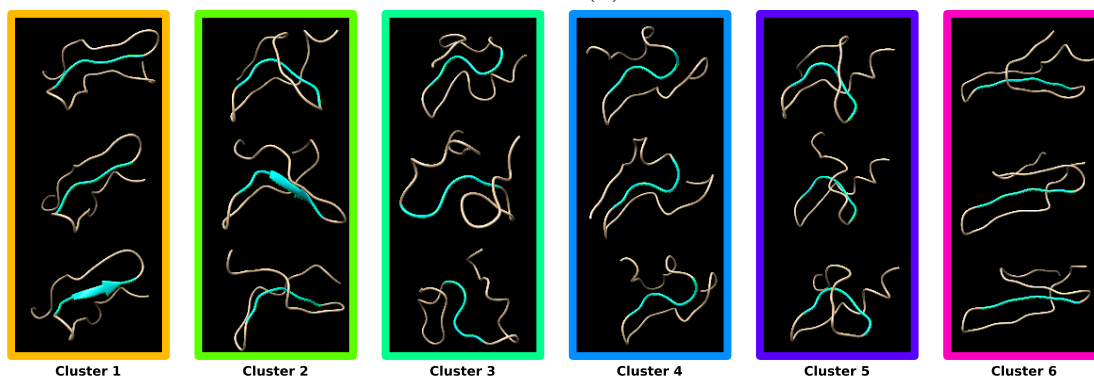


(b)

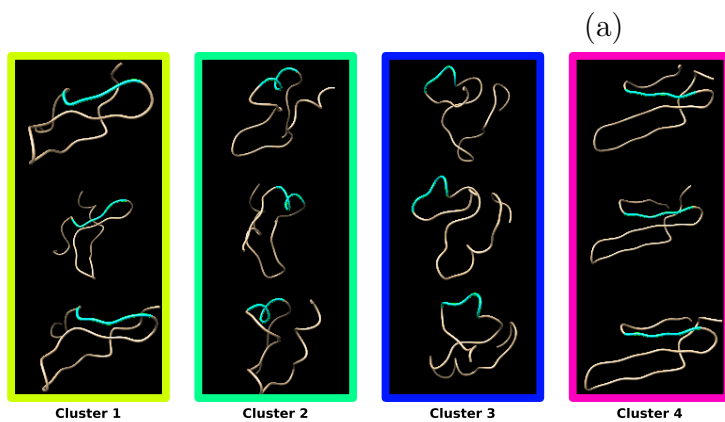
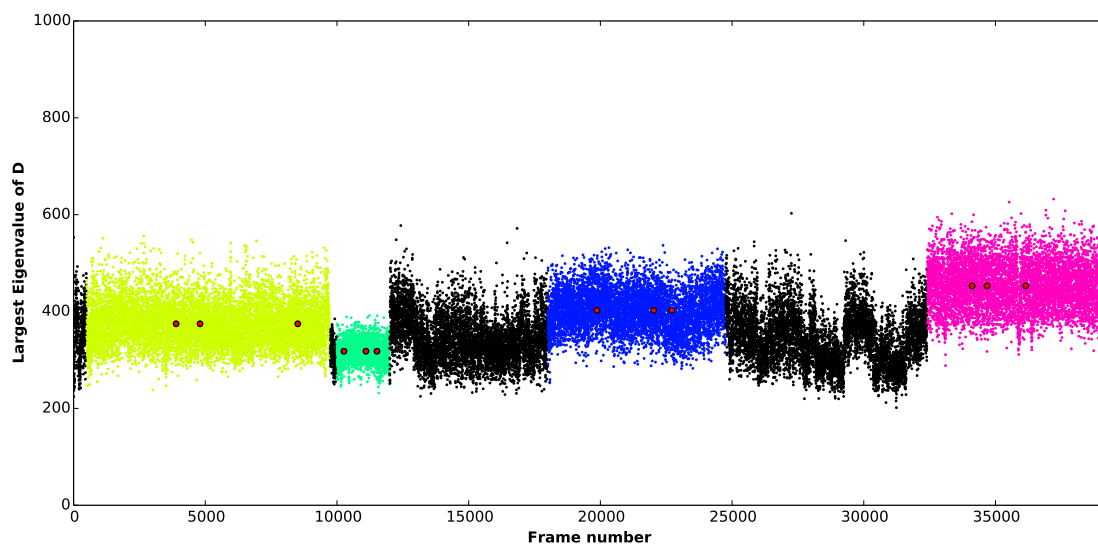
Figure 7  
 Johnston, Zhang, Liwo, Crivelli, and Taufer  
 J. Comput. Chem.



(a)



(b)  
Figure 8  
Johnston, Zhang, Liwo, Crivelli, and Taufer  
J. Comput. Chem.



(b)  
Figure 9  
Johnston, Zhang, Liwo, Crivelli, and Taufer  
J. Comput. Chem.

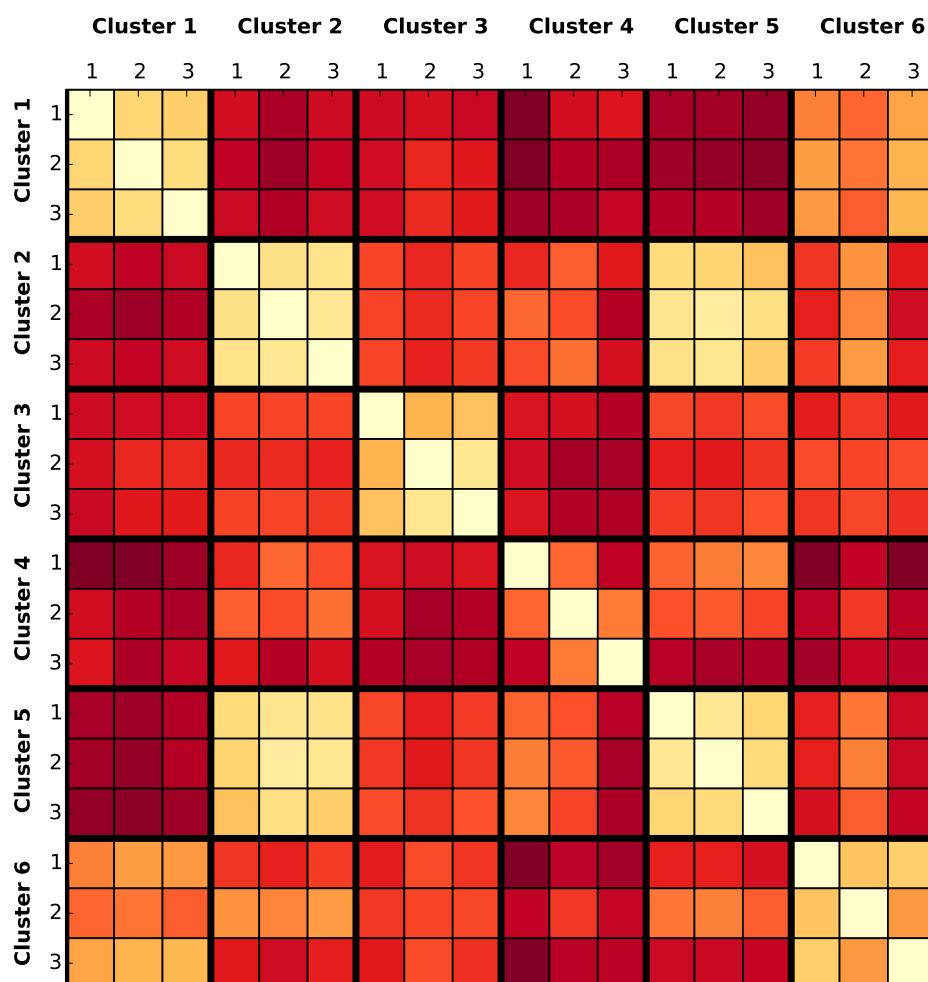


Figure 10  
 Johnston, Zhang, Liwo, Crivelli, and Taufer  
 J. Comput. Chem.

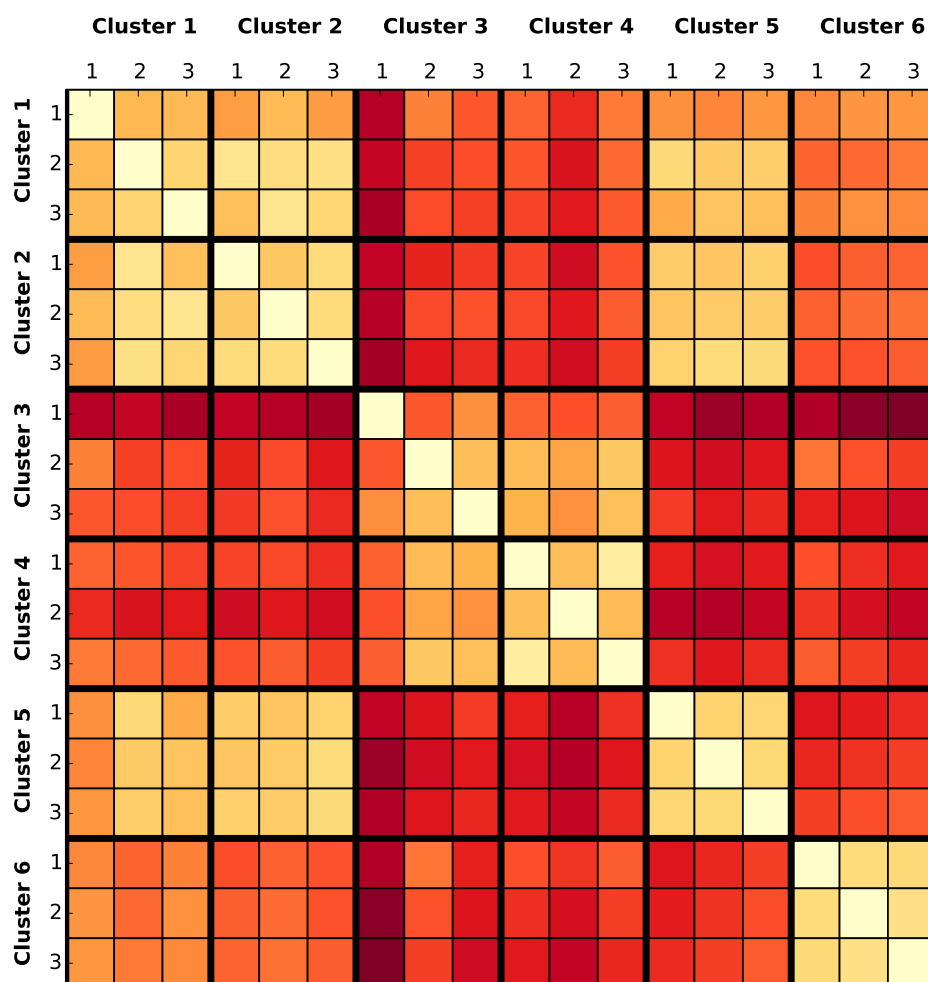


Figure 11  
 Johnston, Zhang, Liwo, Crivelli, and Taufer  
 J. Comput. Chem.

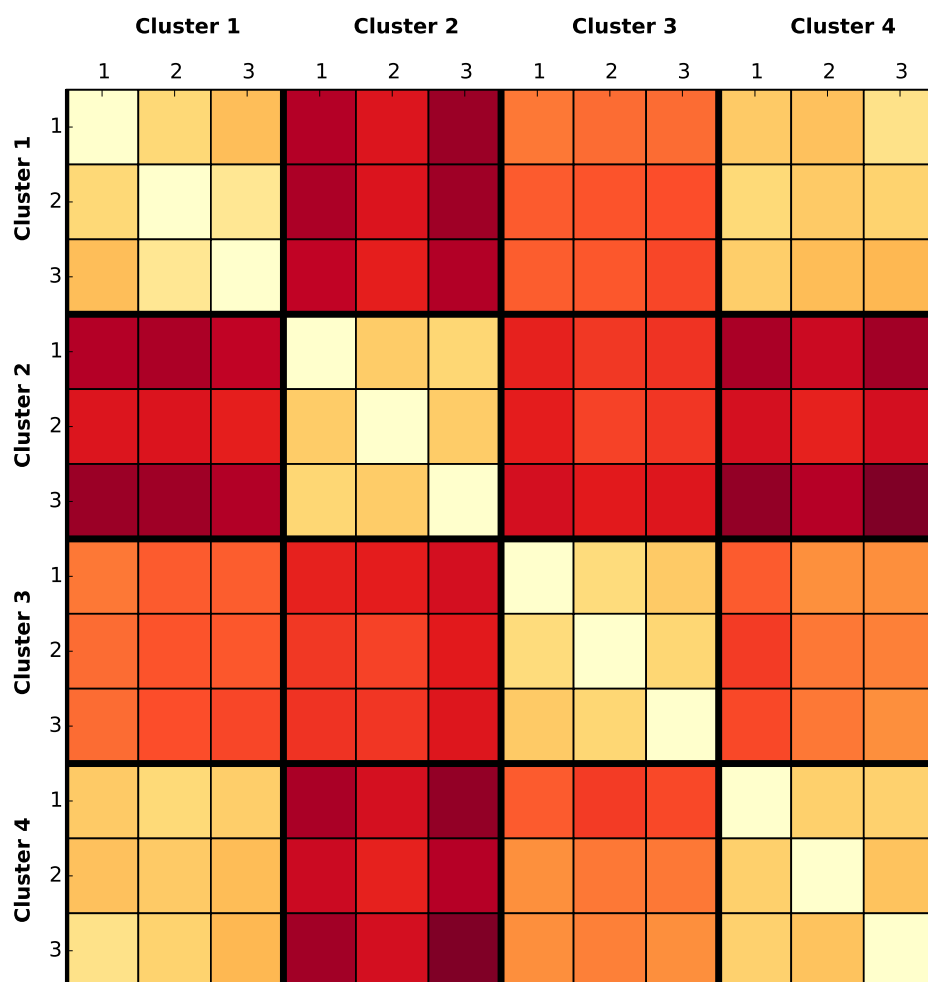
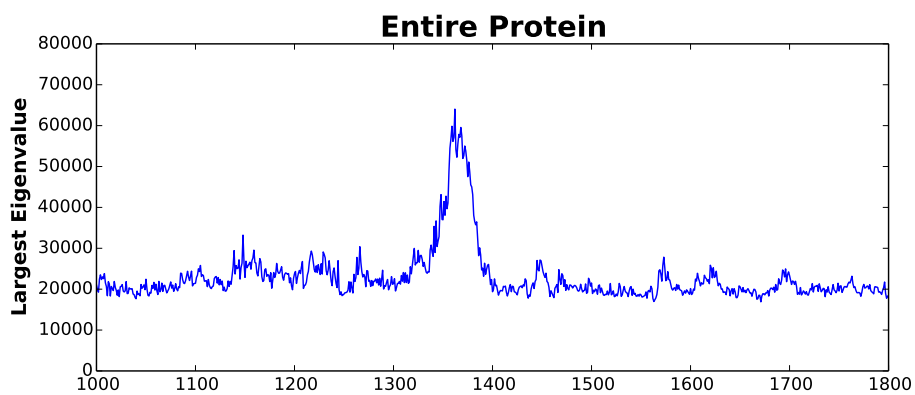
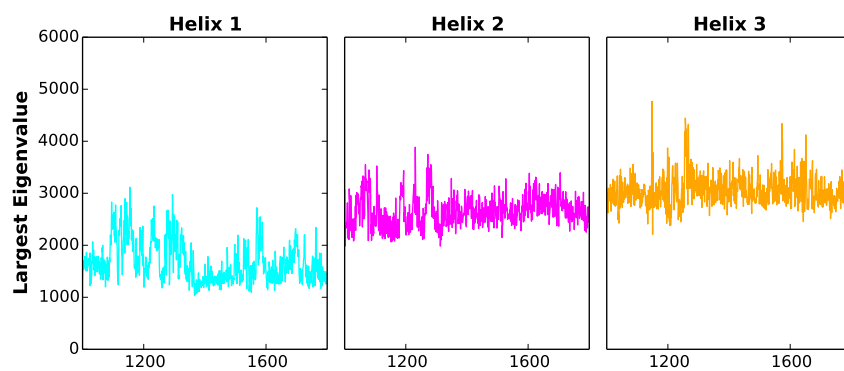


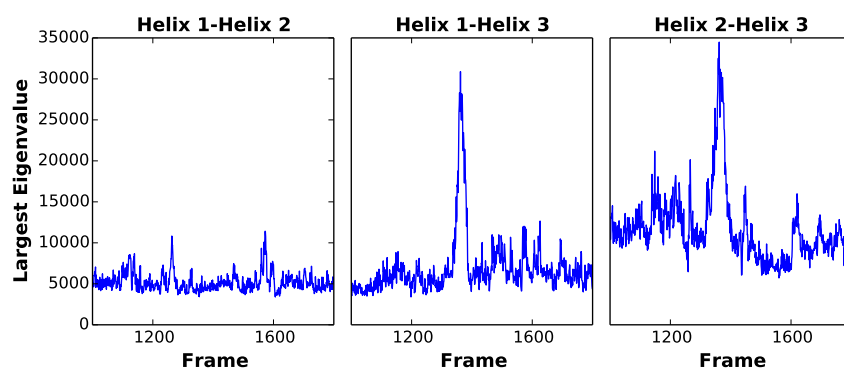
Figure 12  
 Johnston, Zhang, Liwo, Crivelli, and Taufer  
 J. Comput. Chem.



(a)



(b)



(c)

Figure 13  
 Johnston, Zhang, Liwo, Crivelli, and Taufer  
 J. Comput. Chem.

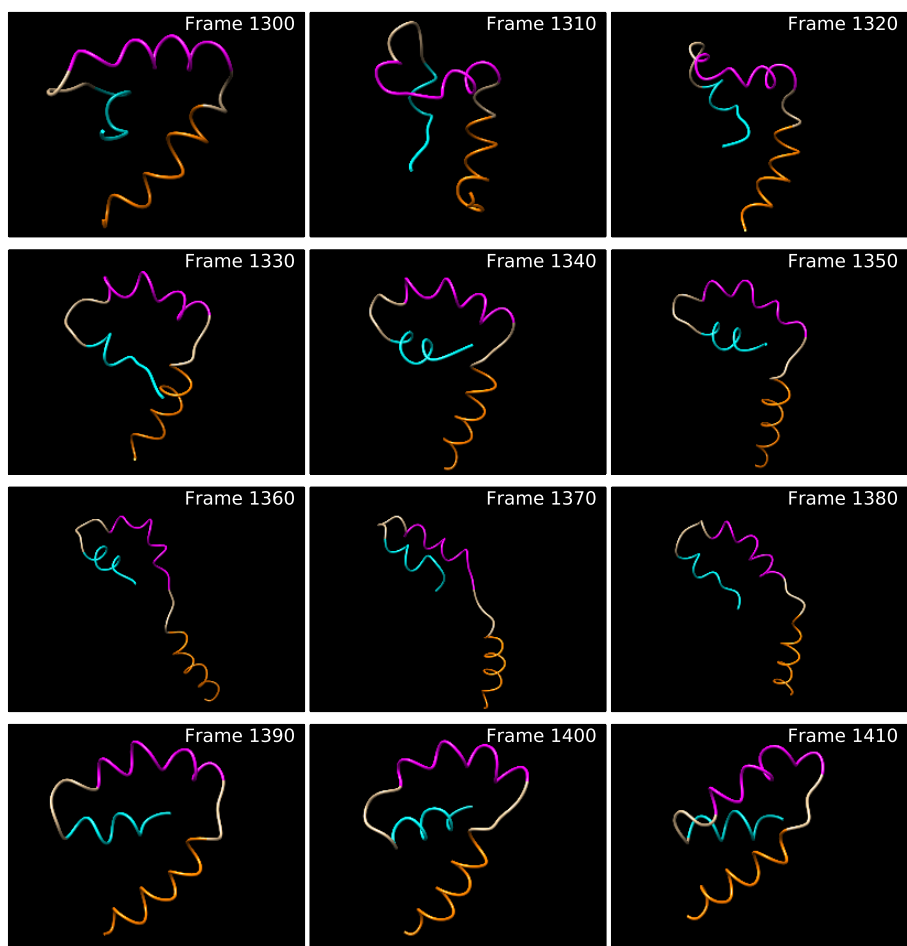


Figure 14  
Johnston, Zhang, Liwo, Crivelli, and Taufer  
*J. Comput. Chem.*